iJETRM
INTERNATIONAL JOURNAL OF ENGINEERING TECHNOLOGY RESEARCH & MANAGEMENT (IJETRM)
https://ijetrm.com/

MULTI-SCALE SPATIO-TEMPORAL VARIABILITY AND TRENDS OF RAINFALL EROSIVITY IN SOUTH-EASTERN NIGERIA FROM HOURLY SATELLITE-DERIVED RAINFALL

J.O. Onyeka,
L.E. Obi,
S.C. Anyanwu,
Department of Civil Engineering, Faculty of Engineering,
Imo State University, Owerri, Nigeria
nopsoftinc@yahoo.com

ABSTRACT
Rainfall erosivity is the climatic driver of water erosion and gully development in South-Eastern Nigeria, yet sub-daily erosivity estimates for the region are scarce. This study derived daily, monthly and annual erosivity indices for Abakaliki, Awka, Enugu, Owerri and Umuahia from 903,600 hourly NASA POWER rainfall records (2005–2025). An hourly-intensity erosivity index (EIh), the Modified Fournier Index (MFI) and the Rainfall Anomaly Index (RAI) were computed; trends were assessed by ordinary least squares and the Mann–Kendall test; station differences were tested by one-way ANOVA; and the mean annual R-factor was interpolated by ordinary kriging and inverse distance weighting (IDW). Erosivity followed the West African Monsoon cycle, being negligible in December–February and peaking between July and October. Annual EIh increased at all five stations, whereas annual rainfall decreased at Abakaliki, Enugu and Umuahia, indicating a shift towards more intense storms rather than greater totals. RAI ranged from +7.10 (2007) to −3.89 (2021) at Abakaliki, revealing strong interannual variability. Ordinary kriging (leave-one-out $R^2 = 0.605$) outperformed IDW ($R^2 \approx 0$) and revealed a south-west to north-east gradient, with Owerri highest and Abakaliki lowest. The results support season-targeted erosion control and provide a regional erosivity baseline for Revised Universal Soil Loss Equation applications.

Keywords:
Rainfall erosivity, Modified Fournier Index, Rainfall Anomaly Index, trend analysis, ordinary kriging, NASA POWER, South-Eastern Nigeria

INTRODUCTION
Soil erosion by water is among the most serious environmental and economic problems in South-Eastern Nigeria, where gully systems threaten farmland, roads and settlements. Rainfall is the primary driver of this process: raindrop impact detaches soil particles and the resulting runoff transports them downslope [1]. The capacity of rainfall to cause erosion—rainfall erosivity—is represented by the R-factor in the Universal Soil Loss Equation (USLE) and its revised form (RUSLE), and it is widely regarded as the best single climatic predictor of erosive potential [2, 3, 4].

The standard R-factor is the sum of storm EI_{30} values, the product of storm kinetic energy and maximum 30-min intensity. Computing it requires continuous pluviograph records at sub-hourly resolution, which are rare across West Africa. Studies in Nigeria have therefore relied on daily or monthly rainfall, using empirical relationships such as the Modified Fournier Index [5, 6, 7, 8]. Global and continental assessments have also highlighted Africa as a region of very high but poorly constrained erosivity [9, 10, 11].

Satellite and reanalysis rainfall products now offer spatially complete, hourly records that can partly fill this gap. Higher temporal resolution generally improves erosivity estimates relative to daily or monthly data [12, 13], and hourly records have been used to map erosivity at national scale elsewhere [14]. For South-Eastern Nigeria, however, no study has combined hourly-resolution erosivity with trend testing and geostatistical mapping.

This study therefore aimed to: (i) derive daily, monthly and annual erosivity indices for five stations in South-Eastern Nigeria from hourly satellite-derived rainfall; (ii) characterise their seasonal and interannual variability using the EIh, MFI and RAI; (iii) assess trends in rainfall and erosivity between 2005 and 2025; and (iv) map the spatial distribution of mean annual erosivity and evaluate kriging against IDW.

 © Author(s) | CC BY 4.0 International License.

iJETRM
INTERNATIONAL JOURNAL OF ENGINEERING TECHNOLOGY RESEARCH & MANAGEMENT (IJETRM)
https://ijetrm.com/

MATERIALS AND METHODS

2.1 Study area

South-Eastern Nigeria covers about 76,358 km² east of the lower Niger and south of the Benue valley, between latitudes 4°N and 7°N and longitudes 7°E and 9°E. The relief comprises plains and lowlands, cuesta landscapes and highlands. The climate is controlled by the seasonal migration of the Inter-Tropical Discontinuity (ITD), which brings a long wet season from April to July, a short break in August and a second wet season from September to October. The most erosive rains are the intense, short-duration storms at the start and end of the rainy season. Five soil classes occur: lithosols, young soils on recent deposits, ferruginous tropical soils, ferrallitic soils and hydromorphic soils. The five stations and their land cover and soils are listed in Table 1 and shown in Figure 1.

Table 1: Meteorological stations, land cover and dominant soils

Station	Lat. (°N)	Long. (°E)	Dominant land cover	Dominant soil
Owerri	5.4763	7.0259	Urban expansion, lowland rainforest, agriculture	Sandy loam to sandy clay loam; ferrallitic
Umuahia	5.5320	7.4860	Mixed agriculture, oil palm, fallow, forest remnants	Coastal plain sands; ferrallitic, high clay
Awka	6.2126	7.0712	Urbanising savanna, cropland, built-up	Sandy loam; derived savanna soils
Abakaliki	6.3249	8.1137	Intensive agriculture, grassland, plantations	Vertisols and hydromorphic soils
Enugu	6.5244	7.5086	Built-up, derived savanna, cropland	Acidic soils on Enugu Shale and Ajali formations

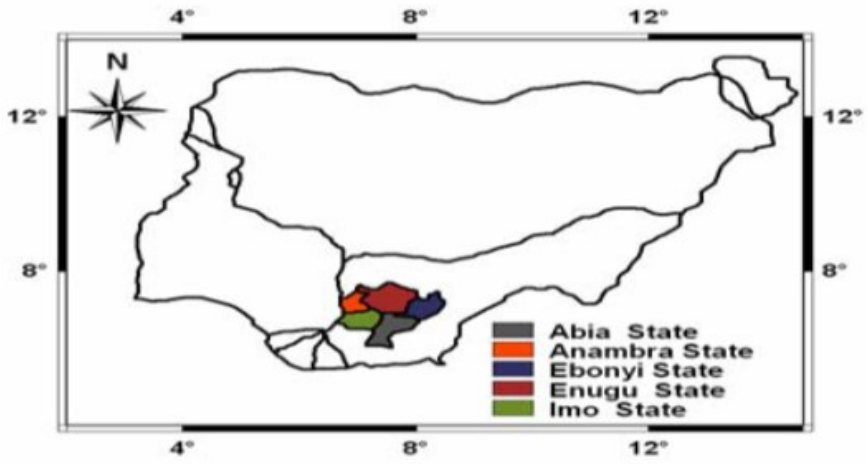


Figure 1: States of South-Eastern Nigeria (after [15]).

2.2 Rainfall data and pre-processing

Hourly rainfall for five stations—Abakaliki, Awka, Enugu, Owerri and Umuahia—was retrieved from the NASA Prediction of Worldwide Energy Resources (POWER) archive for 1 January 2005 to 13 August 2025 (Africa/Lagos time). The dataset comprised 903,600 station-hours with fields for timestamp (YYYYMMDDHH), rainfall (mm h^{-1}) and station. Timestamps were parsed and sorted by station and time, 360 negative values were set to zero as physically implausible, and no duplicate station-hours were found. Hourly records were aggregated to daily totals and daily maximum hourly intensity, then to monthly totals (with rainy-day counts and maximum daily rainfall) and annual totals.

2.3 Erosivity indices

Hourly-intensity erosivity index (EIh). Daily erosivity was computed as

$$EIh_d = P_d \times I_{max,1h} \quad (1)$$

where P_d is daily rainfall (mm) and $I_{max,1h}$ is the maximum hourly intensity of that day (mm h^{-1}). Because 30-min intensities cannot be resolved from hourly data, the maximum hourly intensity was used as a conservative and

 © Author(s) | CC BY 4.0 International License.

iJETRM
INTERNATIONAL JOURNAL OF ENGINEERING TECHNOLOGY RESEARCH & MANAGEMENT (IJETRM)
https://ijetrm.com/

reproducible substitute for I_{30}, and no kinetic-energy term was applied. Monthly and annual indices were obtained by summing EIh_d over the relevant period. All rainfall events above 0 mm were retained so that monthly calibration remained possible.

Modified Fournier Index (MFI). The MFI [16] expresses the concentration of rainfall within the year:

$$MFI = \Sigma_{i=1\ldots12} P_i^2 / P_a \quad (2)$$

where P_i is rainfall in month i and P_a is annual rainfall for the same year.

Rainfall Anomaly Index (RAI). Following a percentile-based form of Van Rooy [17], annual anomalies were computed for each station as

$$RAI_y = +3\ (P_y - \bar{P}) / (P_{90} - \bar{P}) \quad \text{for } P_y > \bar{P} \quad (3)$$

$$RAI_y = -3\ (\bar{P} - P_y) / (\bar{P} - P_{10}) \quad \text{for } P_y < \bar{P} \quad (4)$$

where P_y is annual rainfall in year y, $\bar{P}$ the station mean, and P_{10} and P_{90} the 10th and 90th percentiles of the station record. Positive values indicate wet years and negative values dry years.

2.4 Trend analysis

Annual rainfall and annual EIh at each station were first fitted with an ordinary least-squares (OLS) linear trend, $Y_t = a + bt$, where b is the change per year. Monotonic trends were then tested with the non-parametric Mann–Kendall test [18, 19], whose statistic is

$$S = \Sigma_{k=1\ldots n-1} \Sigma_{j=k+1\ldots n} \operatorname{sgn}(x_j - x_k) \quad (5)$$

and the standardised Z statistic was evaluated at the 5% significance level ($|Z| > 1.96$). Trend magnitude was estimated with Sen's [20] slope estimator. The incomplete 2025 record was excluded from all trend tests.

2.5 Inter-station comparison

Differences in mean annual rainfall among stations were tested by one-way analysis of variance (ANOVA) at $\alpha = 0.05$, followed by Tukey's Honestly Significant Difference (HSD) test to identify which pairs differed and to form homogeneous groups. Model adequacy was checked with residual-versus-fitted, normal probability and residual-versus-order plots in Minitab.

2.6 Spatial interpolation

The mean annual R-factor (mean of annual EIh) at each station was interpolated across the study area by ordinary kriging and IDW (power = 2). Empirical semivariances, $\gamma(h) = \frac{1}{2}(z_i - z_j)^2$, were computed for the ten station pairs using haversine distances. Spherical and exponential models saturated at the distance bound and fitted poorly ($R^2 \approx 0.32$–0.40), so a linear model was adopted:

$$\gamma(h) = 7 \times 10^{-7} + 78{,}041\ h \quad (h \text{ in km}) \quad (6)$$

Kriging weights were obtained by minimising estimation variance subject to the unbiasedness constraint $\Sigma w_i = 1$ [21]. Because five stations cannot support an independent test set, both methods were evaluated by leave-one-out cross-validation (LOOCV) using MAE, RMSE and R^2. IDW powers of 1, 1.5, 2, 3 and 4 were also tested.

RESULTS

3.1 Seasonal regime of rainfall and erosivity

Rainfall followed a well-defined unimodal-to-bimodal monsoon cycle (Figure 2a). It was lowest in December–February, when the dry north-easterly Harmattan suppresses convection, increased from March as the ITD moved north, and remained high from April to October with a slight August break. Maximum monthly rainfall occurred in September–October before a rapid decline in November.

Erosivity tracked rainfall seasonality but with sharper peaks (Figure 2b). EIh was negligible in December–February, rose rapidly from March and was highest between July and October, when large totals coincided with intense storms. The steeper rise in EIh than in rainfall reflects its dependence on intensity as well as amount: a month with moderate rainfall falling in a few intense storms can be more erosive than a wetter month of many low-intensity events. August–October combined the largest totals with the highest intensities and therefore carried the greatest erosion hazard, while March and November were transitional.

 © Author(s) | CC BY 4.0 International License.

iJETRM
INTERNATIONAL JOURNAL OF ENGINEERING TECHNOLOGY RESEARCH & MANAGEMENT (IJETRM)
https://ijetrm.com/

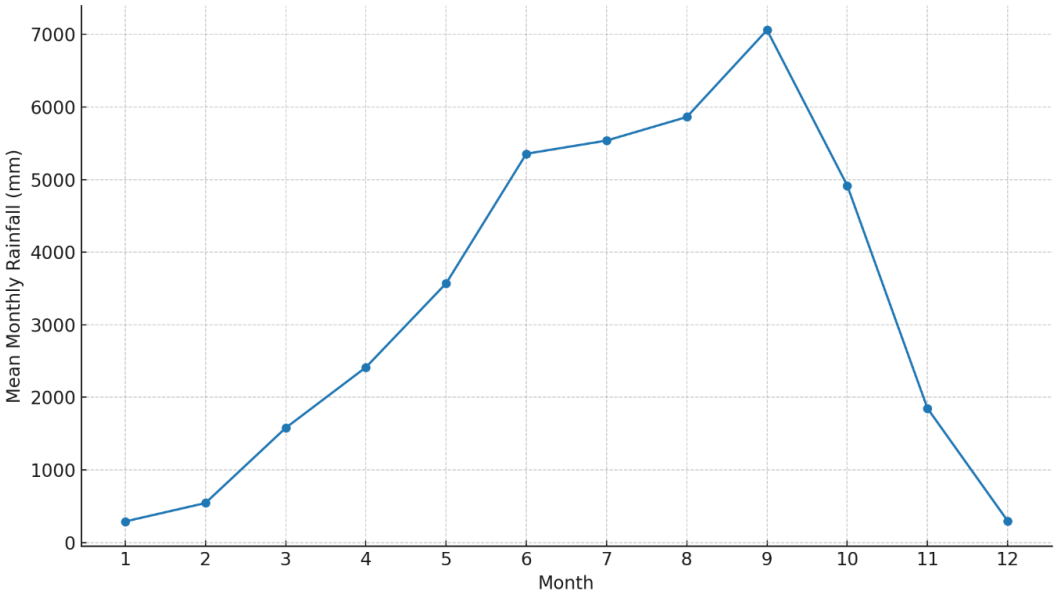


Figure 2a: Monthly climatology of rainfall averaged over the five stations (2005–2025).

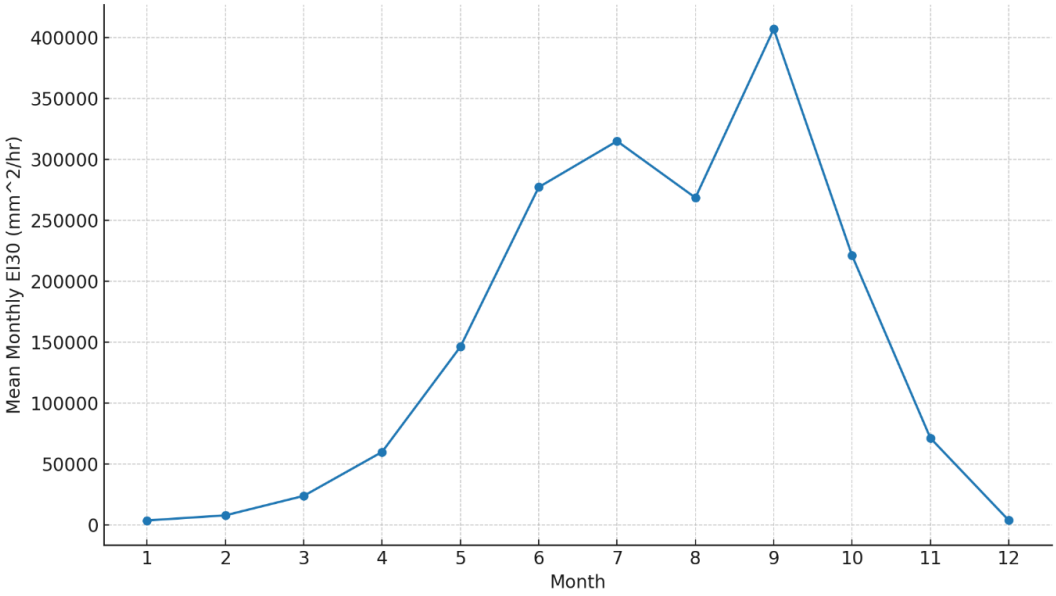


Figure 2b: Monthly climatology of the hourly-intensity erosivity index (EIh) averaged over the five stations.

3.2 Interannual variability: annual EIh, MFI and RAI

Annual rainfall, EIh, MFI and RAI for Abakaliki are given in Table 2 as an illustration; the same indices were computed for all stations. At Abakaliki, 2007 was an extremely wet year (RAI = +7.10) with the highest MFI (7,092), while 2021 was the driest (RAI = −3.89) with the lowest MFI (2,403). Annual EIh did not always follow annual rainfall: 2018 and 2020 had below-average rainfall (RAI = −0.73 and −0.54) but among the highest EIh values of the record, which indicates that a few intense storms rather than total rainfall controlled annual erosivity in those years.

 © Author(s) | CC BY 4.0 International License.

iJETRM
INTERNATIONAL JOURNAL OF ENGINEERING TECHNOLOGY RESEARCH & MANAGEMENT (IJETRM)
https://ijetrm.com/

Table 2: Annual rainfall, EIh, MFI and RAI at Abakaliki (2005–2021)

Year	Annual rainfall (mm)	Annual EIh	MFI	RAI
2005	35,503	966,980	5,007	1.25
2006	40,552	1,240,165	6,261	3.00
2007	52,424	1,875,081	7,092	7.10
2008	33,271	587,592	4,243	0.48
2009	28,334	450,184	3,187	−1.05
2010	41,522	1,080,024	4,820	3.34
2011	40,032	800,614	5,485	2.82
2012	39,220	819,201	4,877	2.54
2013	33,622	614,210	3,886	0.60
2014	26,505	505,168	3,319	−1.59
2015	31,685	1,138,757	4,180	−0.06
2016	37,877	1,181,906	5,184	2.08
2017	32,988	1,561,544	4,444	0.39
2018	29,409	2,026,656	4,275	−0.73
2019	27,428	1,050,962	4,567	−1.32
2020	30,039	2,160,877	4,955	−0.54
2021	18,744	333,917	2,403	−3.89

Station mean annual rainfall $\bar{P}$ = 31,872 mm; P_{10} = 21,739 mm; P_{90} = 40,552 mm.

3.3 Trends in annual rainfall and erosivity

Annual rainfall trends differed among stations (Table 3; Figure 3). Rainfall declined at Abakaliki (−1,031 mm yr^{-1}, R^2 = 0.59), Enugu (−560 mm yr^{-1}, R^2 = 0.21) and Umuahia (−245 mm yr^{-1}, R^2 = 0.04), and increased slightly at Owerri (+375 mm yr^{-1}) and Awka (+145 mm yr^{-1}), the latter with negligible explained variance. In contrast, annual EIh increased at all five stations, by between 36,211 (Abakaliki) and 93,992 (Owerri) units yr^{-1}. The low R^2 of the EIh trends (0.09–0.13) shows that linear trends explain little of the large interannual variance. The consistent sign of the EIh trends despite falling rainfall at three stations nevertheless points to an increase in storm intensity rather than in rainfall amount.

Table 3: Linear (OLS) trends in annual rainfall and annual EIh, 2005–2025

Station	Rainfall slope (mm yr^{-1})	R^2 (rainfall)	EIh slope (units yr^{-1})	R^2 (EIh)
Abakaliki	−1,031	0.592	+36,211	0.126
Awka	+145	0.007	+79,645	0.105
Enugu	−560	0.213	+45,608	0.095
Owerri	+375	0.042	+93,992	0.125
Umuahia	−245	0.039	+46,873	0.088

n = 21 years per station. [Recompute excluding 2025 and after rescaling.]

 © Author(s) | CC BY 4.0 International License.

iJETRM
INTERNATIONAL JOURNAL OF ENGINEERING TECHNOLOGY RESEARCH & MANAGEMENT (IJETRM)
https://ijetrm.com/

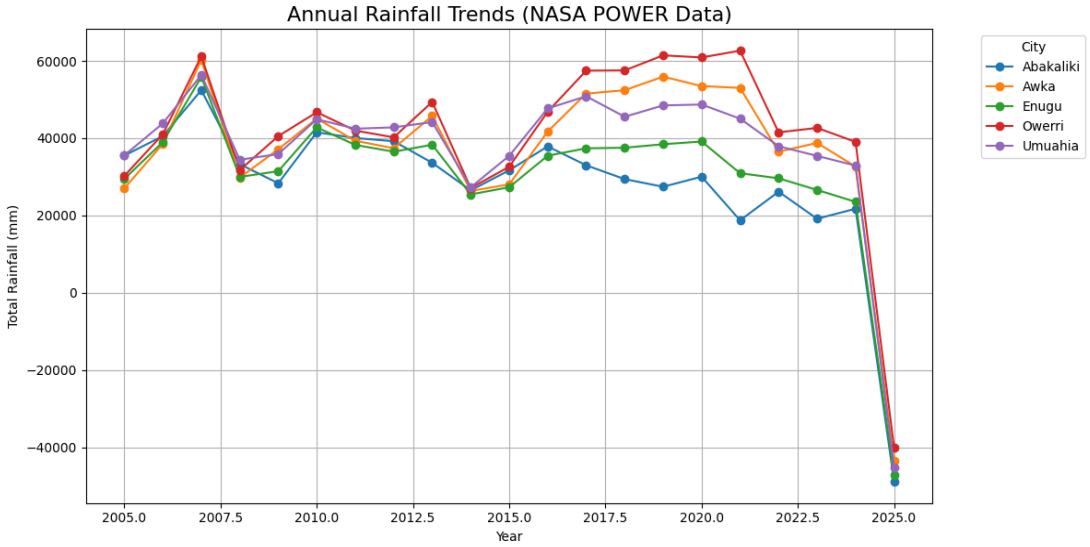


Figure 3: Annual rainfall at the five stations, 2005–2025. The 2025 value is a partial year and is excluded from trend tests.

3.4 Spatial distribution of mean annual erosivity

Mean annual R-factor ranged from 181,095 at Abakaliki to 387,181 at Owerri (Table 5). In leave-one-out cross-validation, ordinary kriging explained 60.5% of the variance (MAE = 44,679; RMSE = 46,429), whereas IDW performed no better than the mean of the remaining stations ($R^2 = -0.001$; MAE = 70,274; RMSE = 73,893). Kriging thus reduced MAE and RMSE by about 36% and 37%. The best IDW power (3) still reached only $R^2 = 0.041$, confirming that the gain came from kriging's use of the fitted spatial-correlation structure rather than a poorly chosen IDW power.

Table 5: Mean annual R-factor and leave-one-out predictions by ordinary kriging and IDW

Station	Observed	Kriging (LOO)	IDW, p = 2 (LOO)
Owerri	387,181	318,111	286,168
Awka	327,844	289,155	269,292
Umuahia	292,268	326,540	330,913
Enugu	220,144	257,194	281,787
Abakaliki	181,095	225,409	272,612
MAE	–	44,679	70,274
RMSE	–	46,429	73,893
R^2 (LOOCV)	–	0.605	−0.001

Both surfaces reproduced a south-west to north-east gradient, with erosivity highest around Owerri and lowest towards Abakaliki and Enugu (Figure 4). Kriging produced smooth contours, whereas IDW created the characteristic "bull's-eye" pattern around each station. Kriging standard error was lowest near the stations and increased towards the edges of the domain, which lie outside the convex hull of the network.

 © Author(s) | CC BY 4.0 International License.

iJETRM
INTERNATIONAL JOURNAL OF ENGINEERING TECHNOLOGY RESEARCH & MANAGEMENT (IJETRM)
https://ijetrm.com/

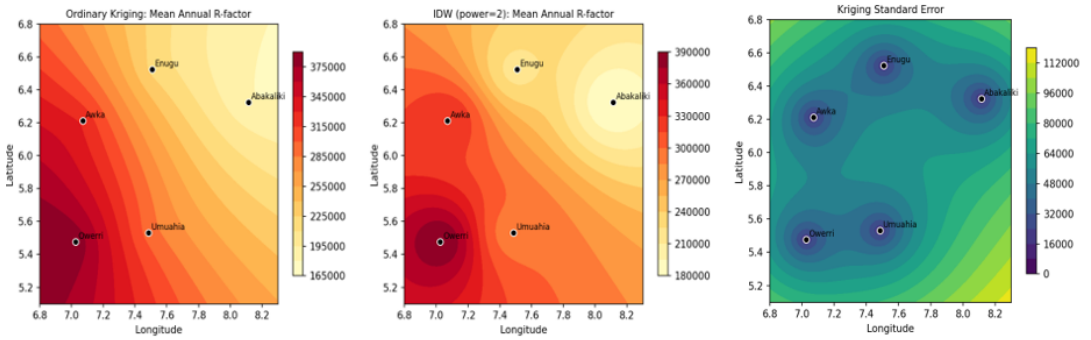


Figure 4: Mean annual R-factor interpolated by (a) ordinary kriging and (b) IDW (power = 2), and (c) kriging standard error.

3.5 Inter-station differences in annual rainfall

One-way ANOVA showed that mean annual rainfall differed significantly among stations ($F = 18.76$, $p < 0.001$; Table 6). Tukey's HSD test separated the stations into a higher-rainfall group (Enugu, Umuahia, Owerri) and a lower-rainfall group (Onitsha, Awka, Abakaliki). Owerri and Umuahia did not differ significantly ($p = 0.288$), nor did Awka, Onitsha and Abakaliki. Residual plots showed no pattern against fitted values or observation order and approximately normal residuals, so the ANOVA assumptions were reasonably satisfied.

Table 6: One-way ANOVA of mean annual rainfall among stations

Source	DF	Adj SS	Adj MS	F	p
Station	5	452,000	90,400.0	18.76	< 0.001
Error	54	260,000	4,814.8		
Total	59	712,000			

[Rerun on the five-station NASA POWER dataset]

DISCUSSION

4.1 Seasonality and implications for conservation

The concentration of erosivity between July and October agrees with the West African Monsoon regime and with earlier Nigerian studies based on daily and monthly rainfall [5, 6]. Because most annual erosivity falls within a few months, conservation measures—mulching, cover cropping, contour farming, terracing and drainage maintenance—should be in place before the onset of the rains. Land prepared without cover during the early wet season is exposed to intense storms on bare soil. Earthworks and slope re-vegetation should likewise avoid the late-season months, when large totals coincide with frequent intense events.

4.2 Rising erosivity with stable or falling rainfall

The most notable result is that annual EIh increased at every station while rainfall decreased at three. This decoupling suggests that rainfall is becoming more concentrated in intense events, consistent with global evidence that precipitation extremes are intensifying even where totals change little [22, 23]. Similar increases in erosivity have been reported in China and Europe [24, 25]. The low explanatory power of the linear trends, however, means the signal should be confirmed with non-parametric tests, longer records and, ideally, change-point analysis of extremes and an assessment of large-scale drivers such as ENSO.

4.3 Spatial pattern and the case for kriging

The south-west to north-east gradient follows distance from the Atlantic moisture source, with higher erosivity on the coastal plain around Owerri and lower values towards the Enugu–Abakaliki area. Kriging outperformed IDW because it adapted its weights to this gradient, and it also provided an uncertainty surface that IDW cannot. With only five stations and ten pairs, however, the variogram is itself uncertain; geostatistical practice recommends far more pairs. The map should therefore be regarded as a first regional approximation. Densifying the network with additional gauges or gridded satellite rainfall, and adding covariates such as elevation and distance from the coast through kriging with external drift, would strengthen it.

4.4 Limitations

Three limitations apply. First, the EIh uses maximum hourly rather than 30-min intensity and contains no kinetic-energy term, so it is a relative index rather than a calibrated R-factor; conversion factors between temporal resolutions [13, 12] could be applied once local pluviograph data are available. Second, satellite and reanalysis products tend to smooth intense rainfall peaks relative to well-maintained gauges, so bias correction against

 © Author(s) | CC BY 4.0 International License.

iJETRM
INTERNATIONAL JOURNAL OF ENGINEERING TECHNOLOGY RESEARCH & MANAGEMENT (IJETRM)
https://ijetrm.com/

Nigerian Meteorological Agency records is needed. Third, the 20-year record is short for robust climate-trend attribution.

CONCLUSIONS

Hourly NASA POWER rainfall for five stations in South-Eastern Nigeria (2005–2025) was used to derive multi-scale erosivity indices and to examine their variability, trends and spatial pattern. Erosivity was strongly seasonal, concentrated between July and October and negligible from December to February. Annual erosivity increased at all five stations while rainfall declined at Abakaliki, Enugu and Umuahia, suggesting intensifying storms. Interannual variability was large, with Abakaliki RAI ranging from +7.10 to −3.89. Ordinary kriging (LOOCV $R^2 = 0.605$) clearly outperformed IDW and revealed a south-west to north-east erosivity gradient, highest at Owerri and lowest at Abakaliki. These results provide a baseline erosivity dataset for RUSLE-based soil-loss assessment and support season- and location-targeted erosion control. Future work should use sub-hourly gauge data for kinetic-energy-based EI_{30}, bias-correct satellite rainfall and densify the spatial network.

DECLARATIONS

Conflict of interest: The authors declare no competing interests.

Data availability: The hourly rainfall data are freely available from the NASA POWER archive (https://power.larc.nasa.gov). Derived daily, monthly and annual erosivity datasets are available from the corresponding author on reasonable request.

Author contributions: [e.g. S.C.A.: conceptualisation, data curation, analysis, writing—original draft; co-authors: supervision, review and editing.]

REFERENCES

1) Nearing, M. A., Yin, S., Borrelli, P., & Polyakov, V. O. (2017). Rainfall erosivity: An historical review. *Catena, 157*, 357–362. https://doi.org/10.1016/j.catena.2017.06.004
2) Wischmeier, W. H., & Smith, D. D. (1978). *Predicting rainfall erosion losses: A guide to conservation planning* (Agriculture Handbook No. 537). USDA.
3) Renard, K. G., Foster, G. R., Weesies, G. A., McCool, D. K., & Yoder, D. C. (1997). *Predicting soil erosion by water: A guide to conservation planning with the Revised Universal Soil Loss Equation (RUSLE)* (Agriculture Handbook No. 703). USDA.
4) Porto, P. (2016). Exploring the effect of different time resolutions to calculate the rainfall erosivity factor R in Calabria, southern Italy. *Hydrological Processes, 30*, 1551–1562. https://doi.org/10.1002/hyp.10737
5) Salako, F. K. (2010). Development of isoerodent maps for Nigeria from daily rainfall amount. *Geoderma, 156*, 372–378. https://doi.org/10.1016/j.geoderma.2010.03.006
6) Okorafor, O. O., Akinbile, C. O., Adeyemo, A., & Egwuonwu, C. C. (2017). Determination of rainfall erosivity index (R) for Imo State, Nigeria. *American Journal of Engineering Research, 6*(2), 1–13.
7) Tom-Cyprain, N., Ekpo, A. E., Orakwe, L. C., & Umobi, C. O. (2020). Spatio-temporal variation in rainfall runoff erosivity over Akwa-Ibom State using annual and monthly precipitation. *Indian Journal of Engineering, 19*(15), 272–278.
8) Ekpo, A. E., Orakwe, L. C., & Nwachukwu, C. P. (2021). Determination of rainfall erosivity in Akwa Ibom State using Modified Fournier Index. *Journal of Engineering and Applied Sciences, 19*(1), 427–435.
9) Vrieling, A., Sterk, G., & de Jong, S. M. (2010). Satellite-based estimation of rainfall erosivity for Africa. *Journal of Hydrology, 395*, 235–241. https://doi.org/10.1016/j.jhydrol.2010.10.035
10) Vrieling, A., Hoedjes, J. C. B., & van der Velde, M. (2014). Towards large-scale monitoring of soil erosion in Africa: Accounting for the dynamics of rainfall erosivity. *Global and Planetary Change, 115*, 33–43. https://doi.org/10.1016/j.gloplacha.2014.01.009
11) Panagos, P., Borrelli, P., Meusburger, K., Yu, B., Klik, A., Lim, K. J., et al. (2017b). Global rainfall erosivity assessment based on high-temporal resolution rainfall records. *Scientific Reports, 7*, 4175. https://doi.org/10.1038/s41598-017-04282-8
12) Yin, S., Xie, Y., Liu, B., & Nearing, M. A. (2015). Rainfall erosivity estimation based on rainfall data collected over a range of temporal resolutions. *Hydrology and Earth System Sciences Discussions, 12*, 4965–4996. https://doi.org/10.5194/hessd-12-4965-2015
13) Panagos, P., Borrelli, P., Spinoni, J., Ballabio, C., Meusburger, K., Beguería, S., et al. (2016b). Monthly rainfall erosivity: Conversion factors for different time resolutions and regional assessments. *Water, 8*(4), 119. https://doi.org/10.3390/w8040119

 © Author(s) | CC BY 4.0 International License.

iJETRM
INTERNATIONAL JOURNAL OF ENGINEERING TECHNOLOGY RESEARCH & MANAGEMENT (IJETRM)
https://ijetrm.com/

14) Yue, T., Yin, S., Xie, Y., Yu, B., & Liu, B. (2022). Rainfall erosivity mapping over mainland China based on high-density hourly rainfall records. *Earth System Science Data, 14*, 665–682. https://doi.org/10.5194/essd-14-665-2022
15) Arnoldus, H. M. J. (1980). An approximation of the rainfall factor in the Universal Soil Loss Equation. In M. De Boodt & D. Gabriels (Eds.), *Assessment of erosion* (pp. 127–132). Wiley.
16) Van Rooy, M. P. (1965). A rainfall anomaly index independent of time and space. *Notos, 14*, 43–48.
17) Mann, H. B. (1945). Nonparametric tests against trend. *Econometrica, 13*, 245–259.
18) Kendall, M. G. (1975). *Rank correlation methods*. Charles Griffin.
19) Sen, P. K. (1968). Estimates of the regression coefficient based on Kendall's tau. *Journal of the American Statistical Association, 63*, 1379–1389.
20) Goovaerts, P. (1997). *Geostatistics for natural resources evaluation*. Oxford University Press.
21) IPCC. (2013). *Climate change 2013: The physical science basis. Contribution of Working Group I to the Fifth Assessment Report of the Intergovernmental Panel on Climate Change*. Cambridge University Press.
22) Toreti, A., Naveau, P., Zampieri, M., Schindler, A., Scoccimarro, E., Xoplaki, E., et al. (2013). Projections of global changes in precipitation extremes from Coupled Model Intercomparison Project Phase 5 models. *Geophysical Research Letters, 40*, 4887–4892.
23) Wang, Y., Cheng, C., Xie, Y., Liu, B., Yin, S., Liu, Y., & Hao, Y. (2017). Increasing trends in rainfall–runoff erosivity in the source region of the Three Rivers, 1961–2012. *Science of the Total Environment, 592*, 639–648. https://doi.org/10.1016/j.scitotenv.2017.02.235
24) Panagos, P., Ballabio, C., Meusburger, K., Spinoni, J., Alewell, C., & Borrelli, P. (2017a). Towards estimates of future rainfall erosivity in Europe based on REDES and WorldClim datasets. *Journal of Hydrology, 548*, 251–262. https://doi.org/10.1016/j.jhydrol.2017.03.006

 © Author(s) | CC BY 4.0 International License.